

# Tunable metallic-like conductivity in microbial nanowire networks

Nikhil S. Malvankar<sup>1,2</sup>, Madeline Vargas<sup>2,3</sup>, Kelly P. Nevin<sup>2</sup>, Ashley E. Franks<sup>2</sup>, Ching Leang<sup>2</sup>, Byoung-Chan Kim<sup>2†</sup>, Kengo Inoue<sup>2‡</sup>, Tünde Mester<sup>2‡</sup>, Sean F. Covalla<sup>2‡</sup>, Jessica P. Johnson<sup>2‡</sup>, Vincent M. Rotello<sup>4</sup>, Mark T. Tuominen<sup>1\*</sup> and Derek R. Lovley<sup>2\*</sup>

**Electronic nanostructures made from natural amino acids are attractive because of their relatively low cost, facile processing and absence of toxicity<sup>1–3</sup>. However, most materials derived from natural amino acids are electronically insulating<sup>1–6</sup>. Here, we report metallic-like conductivity in films of the bacterium *Geobacter sulfurreducens*<sup>7</sup> and also in pilin nanofilaments (known as microbial nanowires<sup>8,9</sup>) extracted from these bacteria. These materials have electronic conductivities of  $\sim 5 \text{ mS cm}^{-1}$ , which are comparable to those of synthetic metallic nanostructures<sup>2</sup>. They can also conduct over distances on the centimetre scale, which is thousands of times the size of a bacterium. Moreover, the conductivity of the biofilm can be tuned by regulating gene expression, and also by varying the gate voltage in a transistor configuration. The conductivity of the nanofilaments has a temperature dependence similar to that of a disordered metal, and the conductivity could be increased by processing.**

Some bacteria secrete 3–5-nm-wide proteinaceous pilin filaments, which can grow tens of micrometres long and have been proposed to serve as nanowires to transport electrons over long distances through a nanostructured network<sup>8,9</sup>. Because biological proteins are generally considered as electronic insulators<sup>1–6</sup>, understanding electron transport through these natural nanostructures is a fundamental scientific challenge<sup>10</sup>. This understanding has implications for the development of nanobiotechnological applications<sup>1,10</sup> and will provide a unique explanation for a wide range of important phenomena that influence carbon and mineral cycling in soils and sediments, bioremediation, corrosion and anaerobic conversion of organic wastes to methane or electricity<sup>8,9</sup>. Previous studies on microbial nanowires were performed under unnatural conditions and gave contrasting results<sup>8–10</sup>, with the underlying conduction mechanism remaining unclear<sup>10</sup>. To advance the fundamental understanding of conduction in these materials, it is essential to investigate the dependence of electrical properties under several experimental probes, such as temperature<sup>11,12</sup>, and to explore the possibility of tuning the conduction by genetic engineering<sup>1,13,14</sup> or gating in a three-terminal device configuration<sup>13,15</sup>. Moreover, it is important to measure the conductivity at low energy and bias voltages so that the material is probed under ‘natural’ conditions.

To directly investigate *in situ* conductivity, biofilms of the *Geobacter sulfurreducens* strain DL-1<sup>7</sup> were grown in a microbial fuel cell with 10 mM acetate as the electron donor (as described previously<sup>16</sup>), modified so that the anode of the fuel cell, which serves as

the electron acceptor to support growth, was composed of two gold electrodes (as a split anode) separated by a non-conductive gap of 50  $\mu\text{m}$ ,  $\sim 50$  times the length of a cell (Fig. 1a). Medium exiting the anode chamber, which still contained substantial acetate ( $\sim 9 \text{ mM}$ ), was directed through another chamber, serving as a control, that had an identical arrangement of two gold electrodes, except that the electrodes were not connected to the cathode and thus could not serve as an electron acceptor for growth.

As expected<sup>16,17</sup>, the current between the anode and the cathode increased over time with cell growth on the electrodes (Fig. 2a). Confocal laser scanning microscopy (CLSM) revealed that the cells formed a confluent biofilm that spread across the non-conductive gap (Fig. 1b–e). In contrast, there was no growth on the control electrodes (which were not connected to the cathode; Supplementary Fig. S1). If only one of the two anodes was connected to the cathode, a biofilm formed only on that side and did not bridge the gap (Supplementary Fig. S2).

The connection between the anodes and the cathode could be temporarily disrupted to connect the two anodes to electronics for *in situ* measurements of conductance across the non-conducting gap (Fig. 2b). There was substantial d.c. conductance between the two electrodes when the biofilm bridged the gap between the electrodes (Fig. 2c). The conductance increased over time, consistent with the increase in biofilm thickness over time. Meanwhile, a.c. impedance spectroscopy measurements (see Supplementary Information), which avoid potential contributions of redox charge transfer and ion diffusion to measured d.c. conductance, and separate electronic and ionic conductivity, gave comparable estimates of conductance (Fig. 2c and Supplementary Fig. S3). When only one or neither of the electrodes had been connected to the cathode in the control chamber, there was no biofilm bridging the gap and the conductance between the two electrodes was negligibly small and did not change over time (Fig. 2c). Deleting acetate from the media removed the potential for microbial current production, but did not change the biofilm conductivity, confirming that the conductivity measured was not associated with current produced by the microorganisms (Supplementary Fig. S4).

The KN400 strain of *G. sulfurreducens* produces higher current densities than the DL-1 strain<sup>7</sup> and had higher conductivity than the DL-1 strain in two-probe measurements (Fig. 3a and Supplementary Fig. S9). A four-probe method confirmed that the measured conductivity was an intrinsic property of the biofilm and could not be attributed to measurement artefacts due to

<sup>1</sup>Department of Physics, University of Massachusetts, Amherst, Massachusetts 01003, USA, <sup>2</sup>Department of Microbiology, University of Massachusetts, Amherst, Massachusetts 01003, USA, <sup>3</sup>Department of Biology, College of the Holy Cross, Worcester, Massachusetts 01610, USA, <sup>4</sup>Department of Chemistry, University of Massachusetts, Amherst, Massachusetts 01003, USA; <sup>†</sup>Present address: Korea Research Institute of Bioscience and Biotechnology, Yusong-gu, Daejeon 305-806, South Korea (B.C.K.); Interdisciplinary Research Organization, University of Miyazaki, Kiyotake, Miyazaki 889-1692, Japan (K.I.); University of Michigan Medical School and Veterans Affairs Medical Research Centre, Ann Arbor, Michigan 48105, USA. (T.M.); Mascoma Corporation, Lebanon, New Hampshire 03766, USA (S.F.C. and J.P.J.). \*e-mail: tuominen@physics.umass.edu; dlovley@microbio.umass.edu

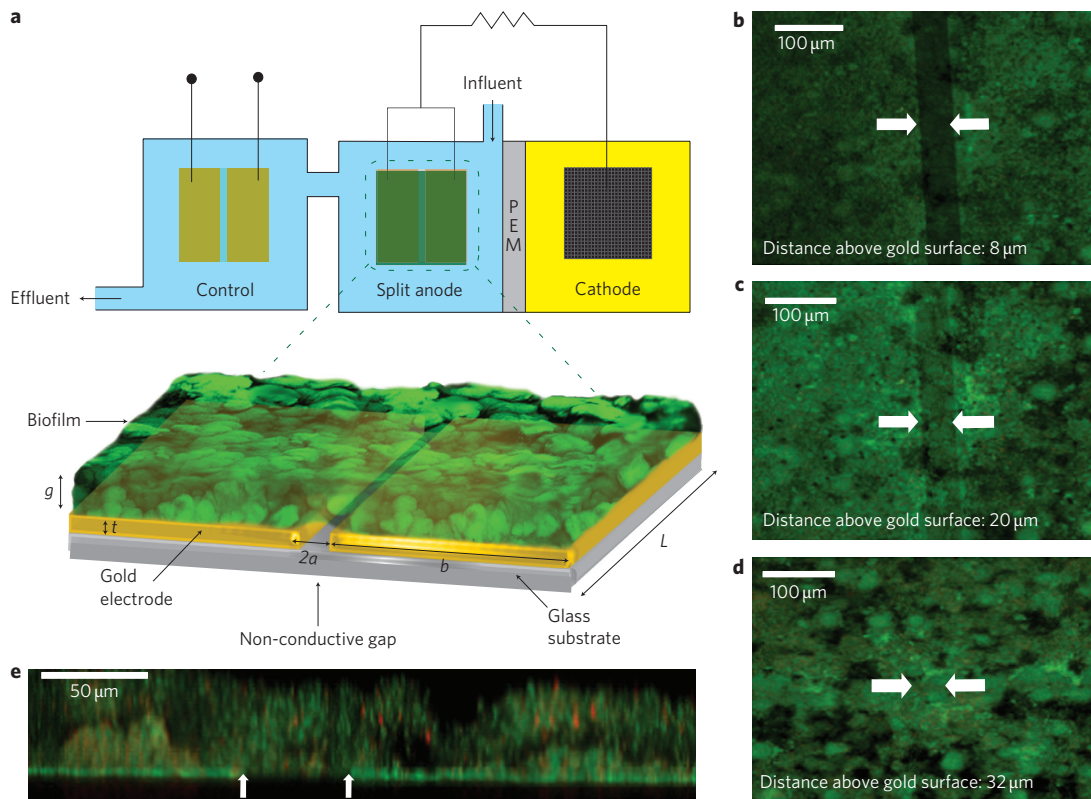


**Figure 1 | Strategy to measure *in situ* biofilm conductivity.** **a**, Schematic of microbial fuel cell with two gold electrodes serving as an anode, separated from the cathode by a proton exchange membrane (PEM). The biofilm grows over the electrodes and the non-conducting gap between the two electrodes. No biofilm forms on the control electrode pair. Gap width  $2a = 50 \mu\text{m}$ , electrode width  $b \approx 1.27 \text{ cm}$ , electrode length  $L \approx 2.54 \text{ cm}$ , electrode thickness  $t \approx 50 \text{ nm}$  and biofilm height  $g$ . **b–e**, Representative fluorescent confocal scanning laser microscopy images of split electrodes. Images were taken when the microbial current was  $0.25 \text{ mA}$  and the biofilm height was  $36 \pm 1.4 \mu\text{m}$ . Gap is indicated by arrows. **b–d**, Top-down confocal image slices of biofilm spanning the non-conductive gap. X–Y image slices (parallel to the electrode surface). Scale bar,  $100 \mu\text{m}$ . **e**, Cross-sectional image of biofilm spanning the non-conductive gap. X–Z image slice through the biofilm, in a direction perpendicular to the surface of the gold anode and across the  $50 \mu\text{m}$  gap. Scale bar,  $50 \mu\text{m}$ .

contacts or electrode polarization<sup>18,19</sup> (Fig. 2d and Supplementary Fig. S5). The conductivity values obtained with the four-probe method were higher than those with the two-probe approach. This can be attributed to the energy level mismatch between the electrodes and the biofilm<sup>18–20</sup>. When two dissimilar materials are put in intimate contact, an energy barrier can form at the interface due to the difference between the materials' work functions and electron affinity that prevents easy electron injection<sup>20</sup>. The four-probe measurements demonstrate that the biofilms are significantly conductive over distances of more than 1 cm because the biofilm was the only possible electronic pathway for the current flow between the current-carrying electrodes spaced 1.25 cm apart.

Using a conformal mapping technique<sup>21</sup>, a conductivity of  $5 \text{ mS cm}^{-1}$  was determined for gap-spanning KN400 biofilms with a height of  $40 \mu\text{m}$ . This is comparable to the conductivity of synthetic organic metallic nanostructures such as polyaniline and polyacetylene<sup>2</sup>.

Biofilms of well-known biofilm formers such as *Pseudomonas aeruginosa* and *Escherichia coli* grew across the non-conducting gap when their preferred electron acceptor, oxygen, was provided (Supplementary Fig. S6). However, the measured conductivity was not significantly greater than the control without a biofilm (Supplementary Fig. S7). This is in agreement with previous reports of biofilms functioning as insulators rather than conductors<sup>4–6</sup>. *Shewanella oneidensis* is reported to have conductive filaments<sup>9,10</sup>, but produces biofilms that are too thin ( $<10 \mu\text{m}$ ) to bridge the non-conducting gap of our apparatus, consistent with previous electrode studies<sup>22</sup>.

The hypothesis<sup>17</sup> that a network of pili nanofilaments might confer conductivity to *G. sulfurreducens* biofilms was evaluated by manipulating pilin abundance in the biofilms. We found a strong correlation between pilin protein and conductivity (Fig. 3a). For example, when the split anodes were not connected to the cathode, but fumarate was provided in the medium as an alternative electron acceptor, a biofilm bridged the non-conductive gap (Supplementary Fig. S8). Conductivity across these biofilms was very small, comparable to controls without biofilms, and consistent with a much lower abundance of pilin protein in the fumarate-grown biofilm (Fig. 3a, Supplementary Fig. S7). The KN400 strain of *G. sulfurreducens*, which has a higher capacity for current production<sup>7</sup>, produced biofilms that had much higher conductivity than the DL-1 strain, and there was more pilin protein in the KN400 biofilm<sup>7</sup> (Fig. 3a, Supplementary Fig. S9). Strain BEST is a strain of *G. sulfurreducens* in which the genes for four of the most abundant outer-surface c-type cytochromes (OmcB, OmcE, OmcS and OmcT) have been deleted<sup>23</sup>. The BEST strain had higher pilin content and higher biofilm conductivity than the DL-1 strain (Fig. 3a, Supplementary Fig. S9). These studies provided an *in situ* demonstration that pili are contributing to biofilm conductivity.

To directly evaluate pili conductivity, pili were sheared off from the live cells of strain KN400 (Fig. 3b), and a concentrated preparation of pili was placed on the split gold electrodes and dried in a desiccator. A similar preparation was made from a control strain of KN400 in which the gene coding for PilA, the pilin structural subunit, was deleted. The pili from the wild-type strain formed an interpenetrating network on the electrode (Fig. 3d), similar to that

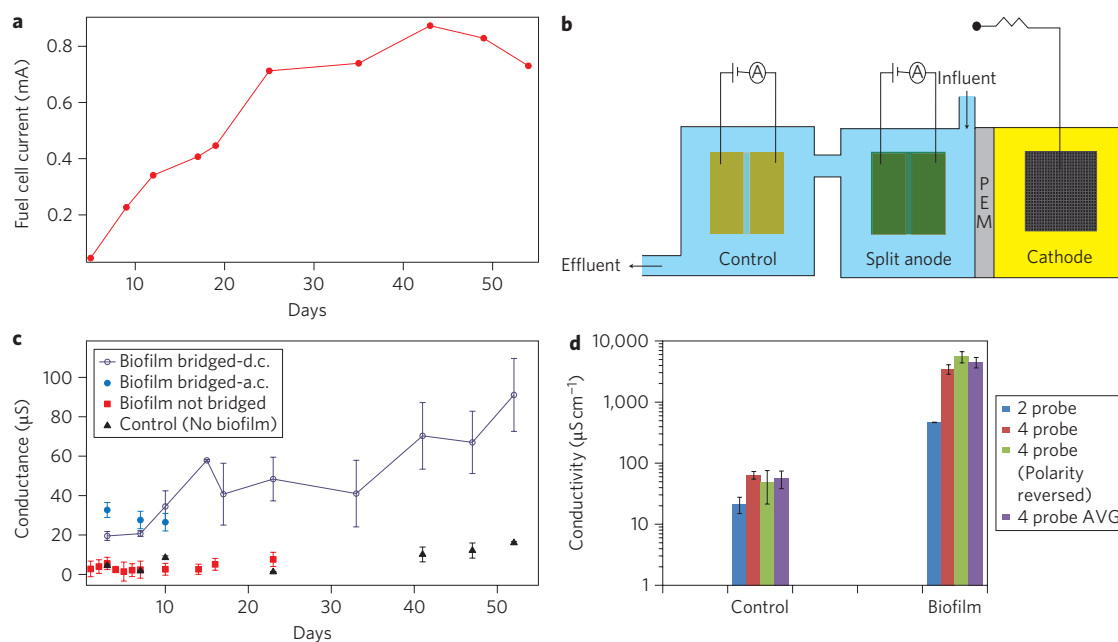


**Figure 2 | Measurement setup and conductance data.** **a**, Representative current produced by the DL-1 strain of *G. sulfurreducens*. **b**, Schematic of conductivity measurements. **c**, Conductance measured across the gap-spanning biofilm as well as measurements from controls in which a biofilm did not span the gap. Error bars indicate the standard deviation (s.d.) of individual measurements for several biofilms ( $n = 5$  for the biofilm bridging the gap and control electrodes,  $n = 2$  for the biofilm not bridging the gap). **d**, Comparison of conductivity measured using two- and four-probe methods. Error bars show s.d. of individual measurements for four biofilms of KN400. AVG indicates the average of forward and reverse polarity conductivity.

present in a biofilm<sup>7</sup> (Fig. 3c), and had a conductivity 10–100 times higher than the preparation of the PilA-deficient mutant or buffer alone (Fig. 3e). Furthermore, denaturing the cytochromes did not affect pili conductivity (Supplementary Fig. S10). Additional control experiments using inorganic metallic nanowires and non-conductive latex nanoparticles yielded expected results, further validating our measurement methodology (Supplementary Fig. S11). The conductivity of pili preparations ( $6 \mu\text{S cm}^{-1}$ ) was comparable to that of peeled biofilms ( $18 \mu\text{S cm}^{-1}$ ). These results confirmed that pili can form a matrix with sufficient conductivity to account for electron flow through biofilms.

Insight into the conduction mechanism in biofilm and pili was obtained by measuring conductivity as a function of temperature. Biofilm measurements were performed with the CL-1 strain of *G. sulfurreducens*, which forms highly cohesive biofilms that, when grown on graphite electrodes, can be peeled off the surface and placed on gold electrodes specifically designed for four-probe measurements. Intact wet biofilms of strain CL-1 exhibited conductance comparable to KN400, with the conductance of peeled or dried biofilms being significantly lower. On cooling from room temperature, biofilm conductivity increased by over an order of magnitude (Fig. 4a). In the case of pili samples, the conductivity increased by three orders of magnitude. An increase in conductivity on cooling is a hallmark of metallic conduction<sup>2,11,12,24</sup>. Notably, the conductivity increased exponentially upon cooling, as expected for high-performance, quasi-one-dimensional organic metals<sup>2,11,12,24</sup>, rather than linearly as in conventional metals, indicating that the conductivity is limited by backscattering from thermal phonons<sup>2,11,12</sup>. In other words, the conductivity begins to decrease exponentially upon heating at temperatures where thermally excited backscattering phonons begin to scatter the charge carriers. For temperatures where the thermal energy ( $k_{\text{B}}T$ ) is much less than the energy of the backscattering phonons ( $\hbar\omega_{\text{b}}$ ), an exponential increase in conductivity on cooling is expressed as<sup>11,12</sup>  $\sigma(T) = \sigma_{\text{m}} \exp(\hbar\omega_{\text{b}}/k_{\text{B}}T)$ . The energy of backscattering phonons calculated from these measurements ( $0.6 \pm 0.2$  eV for biofilm) is

comparable with that observed experimentally for organic metals<sup>24</sup> ( $\hbar\omega_{\text{b}} \approx 0.4$  eV).

At even lower temperatures, the conductivity decreased exponentially with cooling as expected for disordered metals<sup>11,12,24</sup>, which is a signature of the thermally activated hopping mechanism with characteristic Arrhenius dependence<sup>25</sup>  $\sigma(T) = \sigma_0 \exp(-T_0/T)$ . The same conductivity was obtained for heating and cooling. A similar temperature dependence of conductivity has been observed previously for a number of nanostructured organic metals<sup>2,11,12,24–26</sup>. A maximum in conductivity or change in sign of temperature dependence at a crossover temperature  $T^*$  is a key characteristic of many organic metals<sup>12</sup>. The crossover temperature for pili and biofilms ( $T^* \approx 260$ – $270$  K) is close to that reported for organic metals ( $T^* \approx 200$ – $250$  K)<sup>12,24</sup>. The observed conductivity maximum is probably a crossover between two competing mechanisms<sup>2,11,12</sup>: at higher temperatures, conductivity increases with cooling due to intrinsic metallic transport, and at lower temperatures, conductivity decreases with cooling due to the influence of disorder-induced charged traps. Chemical impurities, defects, structural imperfections and inhomogeneities can act as traps to localize electrons<sup>11,12,15</sup>. The activation (detrapping) energy calculated from these measurements ( $k_{\text{B}}T_0$ ) was 1.0 eV for the biofilm, which compares favourably with organic metals<sup>24,25</sup>. In the case of pili samples, the detrapping energy was reduced to 0.85 eV, the conductivity maximum shifted to lower temperatures, and a temperature dependence of conductivity was four orders of magnitude weaker compared to the biofilm (Fig. 4a), all indicating reduced disorder and improved metallic nature<sup>2,11,15</sup>. These studies demonstrate that higher metallic conductivity can be achieved through better processing, and further improvements can enhance the conductivity significantly<sup>11,12</sup>.

We also observed a large gating effect on biofilms, consistent with that previously observed in organic metals<sup>2,15,27</sup>. When electrochemical gating was performed on biofilms in an electrolyte-gated field-effect transistor configuration<sup>2,15,27–29</sup> (Fig. 4b, inset), the conductivity increased in a sigmoidal manner by more than two orders of magnitude with increasing gate potential (Fig. 4b). This response

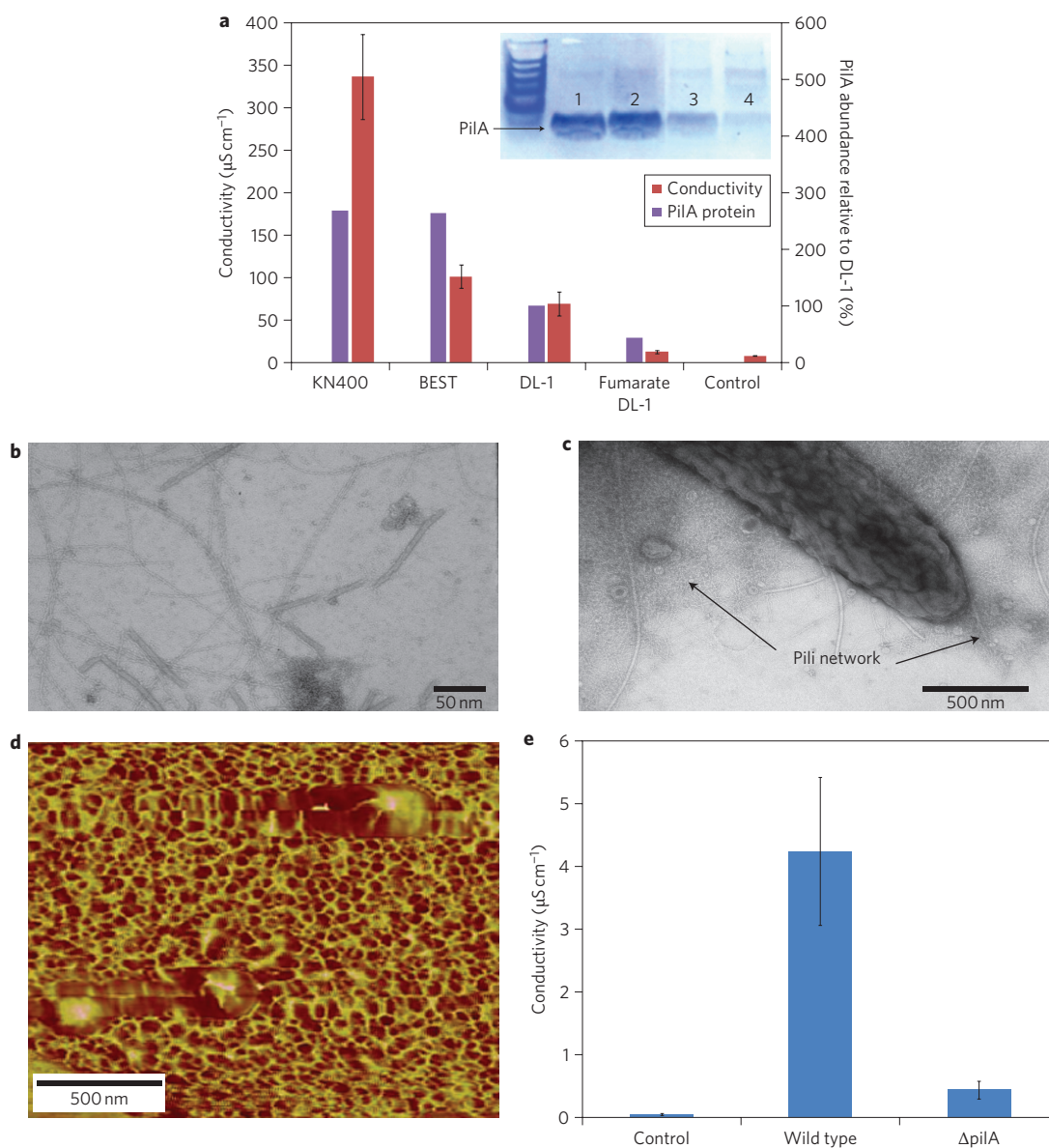


**Figure 3 | Evidence for pili being associated with biofilm conductivity.** **a**, Comparison of conductivity of biofilms of various strains and corresponding structural pilin protein (PilA) in the biofilms. Error bars indicate s.d. PilA expression levels are normalized by PilA expression in DL-1. Correlation coefficient for conductivity and PilA abundance for all DL-1 strains is 0.94. Inset: Western blot analysis of PilA in electrode biofilms. Lane 1, KN400 strain; Lane 2, BEST strain; Lane 3, DL-1 strain; Lane 4, fumarate-grown DL-1 strain. **b**, TEM image of sheared pili nanofilaments. Scale bar, 50 nm. **c**, TEM image of biofilm of strain KN400 grown on split anode. Scale bar, 500 nm. **d**, AFM image of interpenetrating pili filament network after placing pili on electrodes. Scale bar, 500 nm. **e**, Conductivity measurements of filaments of wild-type and PilA mutant of KN400 strain in comparison with control buffer. Data represent mean  $\pm$  s.d. of three biological replicates.

was reversible and no hysteresis was observed. This sigmoidal response is characteristic of organic metals<sup>2,28,29</sup>, and the conductivity plateau at higher gate voltages has been attributed to metallic conduction with a nearly constant density of states<sup>2,27</sup>. At lower gate voltages, the charge carriers can be trapped by the Coulomb potential of anions. However, at higher gate voltages with sufficiently large carrier density, the carrier wavefunctions can overlap and screen the Coulomb attraction between the traps and the carriers, resulting in a transition to the metallic state<sup>15</sup>.

To evaluate whether doping can act as a source of carriers, the conductivity of pili was measured as a function of pH. The conductivity increased by two orders of magnitude with decreasing pH (Supplementary Fig. S12). This pH dependence suggests that pili can be doped by protons, in a manner similar to that observed previously

in organic metals<sup>2,11,30</sup>. Protonation can result in p-type carriers<sup>11,30</sup>, which is consistent with electrochemical gating experiments that have also indicated that the charge carriers in these biomaterials are p-type.

Owing to difficulties in crystallization, the molecular structure of *G. sulfurreducens* pili filaments is not presently known. Recently, semiconductive behaviour has been reported for nanotubes self-assembled from short peptides composed of aromatic residues<sup>1</sup>. We hypothesize that, due to the considerably short length of the pilin protein monomers<sup>8</sup>, the aromatic moieties in pilins<sup>8</sup> might tilt with respect to peptide structures, minimizing the intermolecular distance<sup>3</sup>. Alternatively they might replace the  $sp^3$  carbon atom between the amine and carboxyl groups along the peptide skeleton forming the amide bond<sup>2</sup>, allowing efficient intermolecular electron delocalization in pilin-polymerized filaments, which can result in

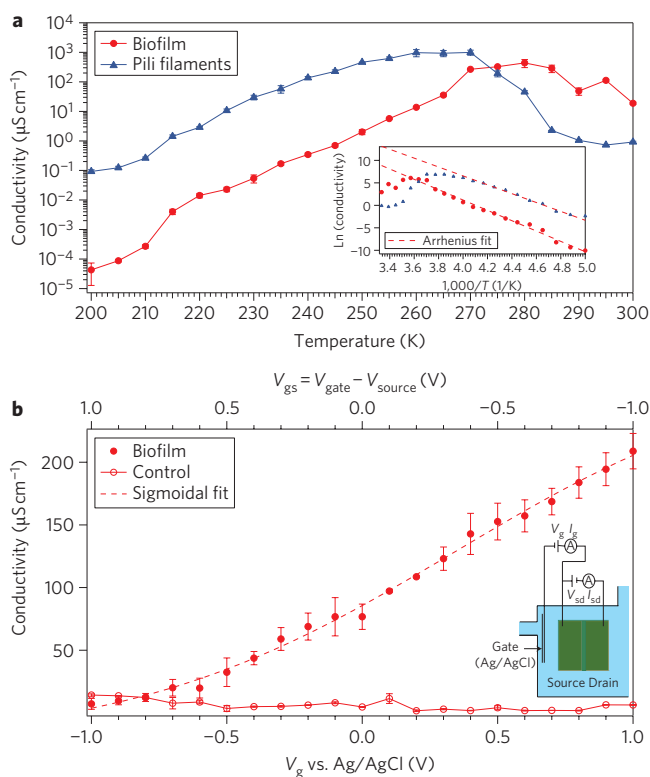


**Figure 4 | Observation of metallic-like nature of conductivity. a,**

Temperature dependence of conductivity of free-standing biofilm formed by *G. sulfurreducens* strain CL-1 and pili filaments of strain KN400 measured with a four-probe method. Error bars represent s.d. Data are representative of several replicates ( $n = 4$  for biofilm;  $n = 3$  for biological replicates for pili). The difference in conductivity between pili and biofilm at 300 K is due to the lower pili concentration required on smaller electrodes for four-probe measurements (see Methods). Control experiments containing media buffer or with biofilm, but not bridging the gap, showed very low conductivity ( $< 1 \times 10^{-2} \mu\text{S cm}^{-1}$  at 300 K; see Fig. 3e) that did not change with temperature. Inset: Arrhenius fit for exponentially decreasing conductivity. **b,** Conductivity of DL-1 biofilm and control measured by electrochemical gating. Error bars show s.d. of individual measurements for two biofilms of strain DL-1. There was no increase in conductivity in the absence of a biofilm. Inset: experimental setup for electrochemical gating: an electrolyte-gated field-effect transistor configuration.  $V_{sd}$  and  $I_{sd}$ : voltage applied and current measured between source and drain electrodes, respectively.  $V_g$  and  $I_g$ : gate voltage applied between reference and source electrodes and gate current measured. Biofilm conductance is calculated as  $G = I_{sd}/V_{sd}$ . Note that the lower scale refers to the voltage at the source electrode with respect to the Ag/AgCl gate electrode (electrochemical convention), whereas the upper scale refers to the voltage at the gate electrode with respect to the source electrode (solid-state transistor convention).

the observed metallic-like conductivity. X-ray diffraction patterns of purified pili revealed sharp peaks superimposed on a broad scattering background indicative of tightly packed crystalline regions dispersed in an amorphous medium<sup>26</sup> (Supplementary Fig. S13). The  $d$ -spacing ( $\sim 3.5 \text{ \AA}$ ) associated with the diffraction peak at  $\sim 25^\circ$  indicates  $\pi$ -orbital overlap and charge delocalization<sup>3,24,26</sup>. Similar  $d$ -spacing has been observed previously in many conductive materials based on aromatic ring stacking<sup>3,24,26</sup>. For example, in organic metal polyaniline, this  $d$ -spacing indicates the face-to-face  $\pi$ - $\pi$  interchain stacking distance between phenyl rings<sup>24,26</sup>. These initial structural data suggest that  $\pi$ - $\pi$  interchain stacking between aromatic amino acids such as phenyl rings in phenylalanine

or phenol rings in tyrosine is present in pili, conferring conductivity to pili. Future structural studies on pili will provide additional insights into the conduction mechanism at the molecular level.

In conclusion, we report metallic-like conductivity in a living, organic material comprising a network of nanofilaments derived from natural amino acids. The demonstrated ability to engineer metallic functionality into natural, self-renewing, nanostructured materials will allow the introduction of new materials and concepts. It may also offer possibilities for overcoming barriers associated with coupling abiotic and biotic materials in nanobioelectronics<sup>1,13</sup> and could provide insights for engineering similar functionalities into synthetic materials<sup>1,14</sup>.

## Methods

**Bacterial strains and culture conditions.** *Geobacter sulfurreducens* strain DL1 (ATCC 51573)<sup>7</sup>, strain KN400<sup>7</sup>, strain BEST<sup>23</sup> and strain CL-1 (a strain that produced a highly cohesive biofilm; Leang *et al.*, in preparation), were obtained from our laboratory culture collection. *Shewanella oneidensis* strain MR-1 (ATCC 700550) was obtained from the American Type Culture Collection. The cultures were maintained at 30 or 25 °C under strictly anaerobic conditions in growth medium supplemented with fumarate (40 mM) as the electron acceptor as described previously with acetate (10 mM) as the electron donor for *G. sulfurreducens*<sup>8,16</sup> or Fe(III) citrate (50 mM) as the electron acceptor and lactate (20 mM) as the electron donor for *S. oneidensis*<sup>22</sup>. *Pseudomonas aeruginosa* strain (obtained from the University of Massachusetts–Amherst microbiology department culture collection) and *E. coli* strain DH5 $\alpha$  (obtained from our laboratory collection) were aerobically grown in M9 media supplemented with 0.1% casamino acids (Difco Lab. USA).

**Biofilm growth on electrodes.** To construct the electrodes, glass slides (2.54 cm  $\times$  2.54 cm) were cleaned ultrasonically using successive rinses of trichloroethylene, acetone and methanol and then blown dry with nitrogen. To achieve an insulating gap in the anode, a 50- $\mu\text{m}$ -diameter tungsten wire was placed on the glass substrate as a deposition mask. For four-probe measurements, electrodes were fabricated using standard photolithography processing. A 40 nm gold film on top of a 10 nm chromium adhesion layer was thermally evaporated on these substrates at  $1 \times 10^{-6}$  mbar and a deposition rate of  $0.1 \text{ nm s}^{-1}$ , producing gold split electrodes with a 50  $\mu\text{m}$  non-conductive spacing. Optical microscopy revealed that the gap was uniform, and resistance measurements confirmed that the electrodes were well insulated from each other ( $G_{\text{gap}} < 1 \times 10^{-10} \text{ S}$ ).

**Microscopy.** Biofilms were examined using CLSM as described previously<sup>16,17</sup>. Biofilms were stained with the LIVE/DEAD BacLight Bacterial Viability Kit (L7012) (Molecular Probes) following the manufacturer's instructions. Anode biofilms were imaged with a Leica TCS SP5 microscope (Leica Microsystems GmbH) with an HXC APO 63 $\times$  (numerical aperture, 0.9) objective, and a minimum of five fields were imaged. Images were processed and analysed with LAS AF software (Leica). A minimum of five random CLSM image stacks were used to determine average biofilm and pili height using the biofilm analysis software Phobia laser scanning microscopy imaging processor (PHLIP). Transmission electron microscopy (TEM) and atomic force microscopy (AFM) were performed as described previously<sup>8</sup>.

**Conductivity measurements (d.c.).** To measure the conductivity under conditions of low energy and bias voltages, a voltage ramp of 0–0.05 V was applied across split electrodes in steps of 0.025 V for two-probe measurements using a source meter (Keithley 2400). For each measurement, after allowing the exponential decay of the transient ionic current, the steady-state electronic current for each voltage was measured every second over a minimum period of 100 s using a Labview data acquisition program (National Instruments). The time-averaged current for each applied voltage was calculated to create the current–voltage ( $I$ – $V$ ) characteristics. For four-probe measurements, a source meter (Keithley 2400) was used to apply a fixed current between the outer of the four electrodes and to measure the potential drop between two inner electrodes<sup>18</sup> by measuring the voltage for each current every second over a period of 100 s after reaching the steady state. An additional high-impedance voltmeter (Keithley 2000) was used to record the output voltage of the current source to calculate conductance<sup>18</sup>. The validity of the four-probe measurements was checked by reversing the polarity of the input current. Forward and reverse currents yielded similar conductivity values, verifying the ohmic contact of the junction (Fig. 2d). For both two- and four-probe measurements, the linearity of the  $I$ – $V$  characteristics was maintained by applying an appropriate low voltage/current. The dissipative power was kept under  $1 \times 10^{-6} \text{ W}$  to eliminate self-heating effects.

**Conductivity measurement in the absence of electron donor (acetate).** When fuel cell current production became stable, the growth medium in the anaerobic chamber was removed under sterile, anaerobic conditions by refilling the chamber with a sterile, anaerobic buffer that did not contain any electron donor. Within a few hours, the current dropped to zero (Supplementary Fig. S4). As described previously<sup>16</sup>, high-performance liquid chromatography (HPLC) was used to confirm that the concentration of acetate was close to zero in the effluent (Supplementary Fig. S4a).

When acetate was again added as the electron donor, fuel cell current production increased rapidly to a maximum and stabilized at levels similar to those observed before medium replacement.

**Conductivity calculation.** Conformal mapping (the Schwarz-Christoffel transformation)<sup>21</sup> was used to calculate biofilm conductivity from the measured biofilm conductance  $G$  (variables defined in Fig. 1a). In the limiting cases  $a < g \ll b$ , the conductivity formula reduces to

$$\sigma = G \frac{\pi}{L} \ln \left( \frac{8g}{\pi a} \right)$$

The conductivity of pili preparations was calculated using the relation<sup>31</sup>

$$\sigma = G \left( \frac{2a}{gL} \right)$$

Thicknesses were determined using confocal microscopy. For conductivity comparisons with controls, the height of the thickest biofilm was used.

**Biofilm characterization.** The biofilms were removed from the gold electrodes using 600  $\mu\text{l}$  of isotonic wash buffer. Collected biomass was immediately frozen with liquid nitrogen and stored at  $-20^\circ\text{C}$ . After thawing, vortexing, sonicating and centrifuging for 5 min at 9,000 r.p.m., supernatants and pellets (cell debris) were collected. Supernatant protein concentration was measured using Quick Start Bradford Dye Reagent (BioRad), and standards were prepared using bovine serum albumin (Sigma). Pellets were suspended in 200  $\mu\text{l}$  deionized water and boiled with 0.5% sodium dodecyl sulphate for 10 min, and protein concentration was determined by the bicinchoninic acid method with bovine serum albumin as a standard (as described previously<sup>7</sup>). To determine the amount of PilA protein in the biofilms, immunoblots were probed with the PilA-specific antiserum as described previously<sup>7</sup>. Immunoreactive bands were visualized with One-Step Western Kit (GeneScript Co) according to the manufacturer's instructions. Each lane was loaded with 8  $\mu\text{g}$  of cell protein. The intensity of the PilA bands was quantified by densitometry using ImageJ software (NIH).

**Pili filament preparation.** To remove pili from the live cells of strain KN400, cells were washed twice in 150 mM ethanolamine buffer (pH 10.5) and vortexed for 2 min to remove pili<sup>32</sup>. Cells were removed by centrifugation. Pili were concentrated and washed by ultracentrifugation at 100,000g or using ammonium sulphate precipitation, and resuspended in ethanolamine buffer<sup>32</sup>. Additional purification was performed using a sucrose gradient method<sup>33</sup> for the cytochrome denaturing experiment. TEM and AFM imaging were used to confirm the presence of pili in filament preparations (Fig. 3b,d). For all conductivity comparisons (Fig. 3e and Supplementary Fig S10), 15  $\mu\text{g}$  of filament protein was placed on the split-gold electrodes and dried in a desiccator for one day. Sucrose gradient treatment yielded a higher room-temperature conductivity ( $\sigma_{\text{dc}}$ (300 K)  $\approx$  1,400 nS; Supplementary Fig. S10) compared to untreated samples ( $\sigma_{\text{dc}}$ (300 K)  $\approx$  1,000 nS; Fig. 3e), indicating an improved metallic nature in more purified samples<sup>21,12</sup>. For haem staining, the cytochrome contents were analysed by 12.5% Tris-tricine denaturing polyacrylamide gel electrophoresis followed by staining with  $N,N,N',N'$ -tetramethylbenzidine as described previously<sup>7</sup>. After sucrose gradient treatment, samples were filtered (filter pore diameter, 0.2  $\mu\text{m}$ ) for additional purification, and 1.14  $\mu\text{g}$  of filament protein was used for temperature experiments (Fig. 4a). The buffer containing pili was equilibrated with aqueous HCl to perform pH experiments<sup>30</sup>.

**Temperature variation experiments.** A physical property measurement system (PPMS-6000, Quantum Design) was used to vary the temperature of a sample stage with an electrode of size 1 cm  $\times$  1.25 cm. A four-probe approach was used to measure conductance. All experiments were performed in vacuum. Best fitting was obtained by testing linear regression ( $R^2$ ) values for various temperature dependences.

**Electrochemical gating.** A source meter (Keithley 2400) was used to apply a voltage  $V_g$  between gate (Ag/AgCl, 3 M KCl reference electrode, BAS) and source-drain electrodes to create the electrolyte gated field effect (Fig. 4b, inset). Gate current  $I_g$  was continuously monitored over the entire experiment. No monotonic dependence of gate current on the measured source-drain current was observed, confirming that the largest part of this ion current does not flow through the biofilm across the gap but originates from the gold electrodes, which were partially covered by electrolyte. Another source meter (Keithley 2400) was used to apply a voltage between source and drain to measure conductance. Igor Pro software (WaveMetrics) was used for data fitting and analysis.

**X-ray diffraction (XRD).** XRD experiments were performed using a PANalytical X'Pert Material Research Diffractometer. The X-ray radiation source was  $\text{CuK}\alpha$  radiation ( $\lambda = 1.5418 \text{ \AA}$ ), and the scattered radiation diffractograms were collected over the range  $2\theta \approx 2-37^\circ$  in a reflection geometry<sup>26</sup>.

Full methods and any associated references are presented in the Supplementary Information.

Received 18 April 2011; accepted 23 June 2011;  
published online 7 August 2011

## References

- Hauser, C. & Zhang, S. Nanotechnology: peptides as biological semiconductors. *Nature* **468**, 516–517 (2010).
- Skotheim, T. A. & Reynolds, J. R. *Handbook of Conducting Polymers* (CRC, 2007).
- Ashkenasy, N., Horne, W. & Ghadiri, M. Design of self-assembling peptide nanotubes with delocalized electronic states. *Small* **2**, 99–102 (2006).
- Dheilly, A. *et al.* Monitoring of microbial adhesion and biofilm growth using electrochemical impedancemetry. *Appl. Microbiol. Biotechnol.* **79**, 157–164 (2008).
- Muñoz-Berbel, X., Muñoz, F. J., Vigués, N. & Mas, J. On-chip impedance measurements to monitor biofilm formation in the drinking water distribution network. *Sens. Actuat. B* **118**, 129–134 (2006).
- Herbert-Guillou, D., Tribollet, B., Festy, D. & Kiéni, L. *In situ* detection and characterization of biofilm in water by electrochemical methods. *Electrochim. Acta* **45**, 1067–1075 (1999).
- Yi, H. *et al.* Selection of a variant of *Geobacter sulfurreducens* with enhanced capacity for current production in microbial fuel cells. *Biosens. Bioelectron.* **24**, 3498–3503 (2009).
- Reguera, G. *et al.* Extracellular electron transfer via microbial nanowires. *Nature* **435**, 1098–1101 (2005).
- Gorby, Y. A. *et al.* Electrically conductive bacterial nanowires produced by *Shewanella oneidensis* strain MR-1 and other microorganisms. *Proc. Natl Acad. Sci. USA* **103**, 11358–11363 (2006).
- Smart, A. G. Two experiments, two takes on electric bacteria. *Phys. Today* **63**, 18–20 (December 2010).
- Heeger, A. J., Sariciftci, N. S. & Namsdas, E. B. *Semiconducting and Metallic Polymers* (Oxford Univ. Press, 2010).
- Kaiser, A. Systematic conductivity behaviour in conducting polymers: effects of heterogeneous disorder. *Adv. Mater.* **13**, 927–941 (2001).
- Noy, A., Artyukhin, A. & Misra, N. Bionanoelectronics with 1D materials. *Mater. Today* **12**, 22–31 (2009).
- Huebsch, N. & Mooney, D. J. Inspiration and application in the evolution of biomaterials. *Nature* **462**, 426–432 (2009).
- Yuen, J. *et al.* Electrochemical doping in electrolyte-gated polymer transistors. *J. Am. Chem. Soc.* **129**, 14367–14371 (2007).
- Nevin, K. P. *et al.* Power output and coulombic efficiencies from biofilms of *Geobacter sulfurreducens* comparable to mixed community microbial fuel cells. *Environ. Microbiol.* **10**, 2505–2514 (2008).
- Reguera, G. *et al.* Biofilm and nanowire production leads to increased current in *Geobacter sulfurreducens* fuel cells. *Appl. Environ. Microbiol.* **72**, 7345–7348 (2006).
- Lange, U. & Mirsky, V. M. Separated analysis of bulk and contact resistance of conducting polymers: comparison of simultaneous two- and four-point measurements with impedance measurements. *J. Electroanal. Chem.* **622**, 246–251 (2008).
- Schwan, H. P. Electrode polarization impedance and measurements in biological materials. *Ann. NY Acad. Sci.* **148**, 191–209 (1968).
- Hadziioannou, G. & Van Hutter, P. F. *Semiconducting Polymers: Chemistry, Physics, and Engineering* 2nd edn, Vol. 2 (Wiley-VCH, 2007).
- Kankare, J. & Kupila, E. L. *In-situ* conductance measurement during electropolymerization. *J. Electroanal. Chem.* **322**, 167–181 (1992).
- Lanthier, M., Gregory, K. B. & Lovley, D. R. Growth with high planktonic biomass in *Shewanella oneidensis* fuel cells. *FEMS Microbiol. Lett.* **278**, 29–35 (2008).
- Voordeckers, J. W., Kim, B.-C., Izallalen, M. & Lovley, D. R. Role of *Geobacter sulfurreducens* outer surface *c*-type cytochromes in reduction of soil humic acid and anthraquinone-2,6-disulfonate. *Appl. Environ. Microbiol.* **76**, 2371–2375 (2010).
- Dallas, P. *et al.* Characterization, magnetic and transport properties of polyaniline synthesized through interfacial polymerization. *Polymer* **48**, 3162–3169 (2007).
- Abthagir, P. S. & Saraswathi, R. Charge transport and thermal properties of polyindole, polycarbazole and their derivatives. *Thermochim. Acta* **424**, 25–35 (2004).
- Lee, K. *et al.* Metallic transport in polyaniline. *Nature* **441**, 65–68 (2006).
- Zotti, G. *et al.* Potential-driven conductivity of polypyrroles, poly-*n*-alkylpyrroles, and polythiophenes: role of the pyrrole nh moiety in the doping-charge dependence of conductivity. *Chem. Mater.* **15**, 4642–4650 (2003).
- Zotti, G. *et al.* Conductivity in redox modified conducting polymers. 2. Enhanced redox conductivity in ferrocene-substituted polypyrroles and polythiophenes. *Chem. Mater.* **7**, 2309–2315 (1995).

29. Lindsay, S. Molecular wires and devices: advances and issues. *Faraday Discuss.* **131**, 403–409 (2006).
30. Chiang, J. C. & MacDiarmid, A. G. 'Polyaniline': protonic acid doping of the emeraldine form to the metallic regime. *Synth. Metals* **13**, 193–205 (1986).
31. Agrell, H., Boschloo, G. & Hagfeldt, A. Conductivity studies of nanostructured TiO<sub>2</sub> films permeated with electrolyte. *J. Phys. Chem. B* **108**, 12388–12396 (2004).
32. Hélaïne, S. *et al.* PilX, a pilus-associated protein essential for bacterial aggregation, is a key to pilus-facilitated attachment of *Neisseria meningitidis* to human cells. *Mol. Microbiol.* **55**, 65–77 (2005).
33. Roine, E. *et al.* Hrp pilus: a hrp-dependent bacterial surface appendage produced by *Pseudomonas syringae* pv. tomato DC3000. *Proc. Natl Acad. Sci. USA* **94**, 3459–3464 (1997).

### Acknowledgements

The authors thank D. Venkataraman, C. Salhouse, M. Aklujkar, J. Nicholson, R. Krotvov, A. Ursache, O. Yavuzcetin and S. Ebru Yalcin for helpful discussions and technical assistance. This research was supported by the Office of Naval Research (grant no. N00014-10-1-0084), the Office of Science (BER), US Department of Energy (award no.

DE-SC0004114 and Cooperative Agreement no. DE-FC02-02ER63446 as well as the NSF Center for Hierarchical Manufacturing (grant no. CMMI-0531171)).

### Author contributions

The experiments were designed by N.S.M., K.P.N. and M.T.T., with suggestions from A.E.F., S.F.C., V.M.T. and D.R.L. N.S.M. performed electrical measurements, X-ray studies and AFM imaging of pili preparations. M.V. prepared and TEM-imaged pilin filaments and performed haem staining. N.S.M., M.V., B.C.K., K.I. and T.M. performed protein measurements. B.C.K. generated the BEST strain. C.L. generated the CL-1 strain and performed the peeling and TEM-imaging of biofilms. A.E.F. and J.P.J. carried out the confocal imaging of biofilms. N.S.M., M.T.T. and D.R.L. analysed the data and wrote the manuscript. All authors discussed the results and commented on the manuscript.

### Additional information

The authors declare no competing financial interests. Supplementary information accompanies this paper at [www.nature.com/naturenanotechnology](http://www.nature.com/naturenanotechnology). Reprints and permission information is available online at <http://www.nature.com/reprints>. Correspondence and requests for materials should be addressed to M.T.T. and D.R.L.